Liu, W., Wen, J., Chao, J., Yin, W., Shen, C., Lai, D., Lin, C.-H., Liu, J., Sun, H., and Chen, Q. 2012. "Accurate and high-resolution boundary conditions and flow fields in the first-class cabin of an MD-82 commercial airliner," *Atmospheric Environment,* 56, 33-44.

Accurate and High-Resolution Boundary Conditions and Flow Fields in the First-Class Cabin of an MD-82 Commercial Airliner

Wei Liu[1], Jizhou Wen[1], Jiangyue Chao[1], Weiyou Yin[1], Chen Shen[1], Daiyi Lai[1], Chao-Hsin Lin[2], Junjie Liu[1], Hejiang Sun[1,*] Qingyan Chen[1,3]

[1]School of Environmental Science and Engineering, Tianjin University, Tianjin 300072, China
[2]Environmental Control Systems, Boeing Commercial Airplanes, Everett, WA 98203, USA
[3]School of Mechanical Engineering, Purdue University, West Lafayette, IN 47907, USA

[*]Email address: sunhe@tju.edu.cn

Abstract

Flow fields in commercial airliner cabins are crucial for creating a thermally comfortable and healthy cabin environment. Flow fields depend on the thermo-fluid boundary conditions at the diffusers, in addition to the cabin geometry and furnishing. To study the flow fields in cabins, this paper describes a procedure to obtain the cabin geometry, boundary conditions at the diffusers, and flow fields. This investigation used a laser tracking system and reverse engineering to generate a digital model of an MD-82 aircraft cabin. Even though the measuring error by the system was very small, approximations and assumptions were needed to reduce the workload and data size. The geometric model can also be easily used to calculate the space volume. A combination of hot-sphere anemometers (HSA) and ultrasonic anemometers (UA) were applied to obtain the velocity magnitude, velocity direction, and turbulence intensity at the diffusers. The measured results indicate that the flow boundary conditions in a real cabin were rather complex and the velocity magnitude, velocity direction, and turbulence intensity varied significantly from one slot opening to another. UAs were also applied to measure the three-dimensional air velocity at 20 Hz, which could also be used to determine the turbulence intensity. Due to the instability of the flow, it should at least be measured for 4 minutes to obtain accurate averaged velocity and turbulence information. It was found that the flow fields were of low speed and high turbulence intensity. This study provides high quality data for validating Computational Fluid Dynamics (CFD) models, including cabin geometry, boundary conditions of diffusers, and high-resolution flow field in the first-class cabin of a functional MD-82 commercial airliner.

Keywords: Airliner Cabin; Cabin geometry; Flow field; Experiment; Diffuser

1. Introduction

Air distributions in commercial airliner cabins are used to maintain thermal comfort and air quality of passengers and crew. These air distributions can control air temperature and air velocity fields and can dilute gaseous and particulate concentrations. Although the aerospace industry has improved thermal comfort and hygiene in aircraft cabins in the past decades (Space et al., 2000), further improvements are needed in the air distribution systems.

According to a review of the state-of-the-art methods for studying air distributions in commercial airliner cabins (Liu et al., 2012), two main methods are available for the study and design of air distribution in an aircraft cabin: experimental measurements and numerical simulations. Experimental studies are usually thought to be more reliable but they are often very expensive and time consuming, so measurements are mainly used to provide data for validating numerical simulations (Garner et al., 2003; Mo et al., 2003). A validated numerical tool can then be used to analyze many scenarios for achieving the best design at a low cost.

The validation of a numerical tool requires accurate geometry, thermo-fluid boundary conditions, and a high-resolution airflow field from a realistic air cabin. Most of the studies have used cabin mockups (Zhang et al., 2009; Günther et al., 2006; Zhang et al., 2005; Sze et al., 2009; Marcus et al., 2010), but these mockups were quite different from real aircraft cabins, especially the duct system and diffusers. As a result, the influence of the differences on the air flow is still unknown. Therefore, it is ideal to use a real plane for obtaining reliable and high quality experimental data.

At present, there are three methods available for obtaining geometric information (Chao et al., 2011). The first one is to convert a CAD model from when the cabin was designed. This method is the most convenient but it contains errors. For example, the geometry of an aircraft cabin may change due to its services and operation, and the original CAD model may not be updated to reflect the changes. The second method is to directly measure the cabin geometry with rulers. Since cabin geometry is very complex and the scale changes dramatically from one component to another, direct measurements could have large errors unless a very dedicated measuring technique is used. The last method is a reverse engineering process that uses a scanning system to obtain key geometric information and inverses the information to form a digital model. Nowadays, the laser tracker system is the most commonly used in data acquisition in terms of the interferometry principle because it can rapidly track the position with accuracy to about a micrometer (Chen et al. 2000). Reverse engineering has been widely used in industry especially for generating a geometrical model of an existing part. So this investigation used this method to obtain accurate geometry of an aircraft cabin.

Accurate boundary conditions are mainly the air velocity, direction, and turbulent information from the diffusers for an isothermal case as most aircraft cabins have very complicated air supply diffusers that make the measurements of the boundary condition very challenging. Zhang et al. (2009) used Hot-Sphere Anemometers (HSA) to obtain the velocity magnitude from the diffusers in a full-scale, twin-aisle section of an aircraft cabin mockup. As the diffusers were small and the inlet air velocity was relatively high, it was very difficult to obtain accurate flow information. This was due to the high velocity gradient near the diffusers. In addition, the HSA could not measure the flow direction. Zhang et al. (2009) estimated this direction by using smoke visualization, but the estimation was not accurate. It is possible to measure the boundary conditions by using optical anemometers. For example, Günther et al. (2006) used a Particle Image Velocimetry (PIV) system to measure the boundary conditions in an empty cabin mockup, but they assumed that the inflow boundary was uniform along the longitudinal direction, so they just measured the boundary conditions at one cross section. In reality, the boundary conditions were not uniform along the longitudinal direction. To measure the velocity distribution along a diffuser with a PIV is very difficult. Zhang et al. (2005) applied Volumetric Particle Streak Velocimetry (VPSV) to measure the flow in a five-row section of a commercial aircraft cabin mockup. Identifying streaks in the inlet flow was very difficult because of the high bubble density and high velocity. Large measurement errors were expected in the inlet airflow jet regions. Although they obtained high quality data for the flow field, the data should be supplemented with accurate boundary conditions.

Liu et al. (2012) summarized many different methods for air distribution measurements. Hotwire and hot-sphere anemometers can provide point-by-point data and have great uncertainties when the air velocity is low (lower than 0.1 m/s). The Particle Tracking Velocimetry (PTV), Particle Streak Velocimetry (PSV), and PIV can only measure in the spaces where a laser light sheet can penetrate. When they were used in an airliner cabin, passengers (typically manikins) and seats would block the laser light sheet, so no flow could be measured in the lower part of the cabin. The Ultrasonic Anemometer (UA) can give three-dimensional, point-by-point airflow information. Zhang et al. (2009) applied UA to measure the flow field in a cabin. The measured data had low resolution because the UA sensor was very expensive, so they used only two UAs in their experiment. If the data resolution is low, many flow features cannot be identified. However, the UA can give accurate velocity and direction at the points measured.

In order to provide high quality data for validating Computational Fluid Dynamics (CFD) models, the objective of this investigation is to obtain accurate cabin geometry, boundary conditions of diffusers, and high-resolution flow field in the first-class cabin of a functional MD-82 commercial airliner.

2. Case Setup

The use of a functional MD-82 airplane can produce the most realistic airflow information in a cabin. Figure 1 shows the schematic model of the first-class cabin in the airplane: 3.28 m (L) × 2.91 m (W) × 2.04 m (H). The cabin contained three rows of seats, three and a half pieces of diffusers, and seven windows on each side. Each air-supply diffuser had 280 linear slots arranged in two rows, as shown in Figure 2. The size of each slot was 22 mm long and 3 mm wide. The air was exhausted from the seven outlets located on each side of the wall near the floor.

The aircraft could supply air through the environmental control system powered by the engines, the auxiliary power unit, and a ground air-conditioning cart. This investigation, however, used only the ground air-conditioning cart that is most economical and can control precisely the supply airflow and temperature. For example, with the air-conditioning cart, the measured flow rate by the constant tracer gas method was 565 ± 15 m^3/h and the supply air temperature was controlled at 20 ± 1 ^oC for the first-class cabin.

The cabin was also further insulated by insulation material that had a thermal resistance of 0.857 $(K \cdot m^2)/W$. The insulation can reduce the temperature swing in the cabin so that isothermal conditions can be maintained during the experiment. The largest temperature difference between the supply and return air was less than 1.5 K during the experiment.

Note that this investigation used a functional aircraft, it represented realistic conditions on ground. The air cabin conditions at cruising height could be different from those on ground, due to a lower cabin pressure and different on the cabin wall surface temperature. Although outside pressure at cruising height could be as low as 0.2 atm, cabin is pressured to have a pressure at least 2000 m above sea level. The difference on the air distribution should not be very large between the cruising and on ground conditions. The surface temperature at cruising height is normally not very low due to the high cruising speed. The authors have measured surface temperature on two large commercial airplanes and found that the interior surface temperature to be comparable to that on the ground as used in this investigation. The case reported in this paper is to provide good data for validating numerical tools. Then the validated numerical tools can be used to study any conditions, including, cruising, takeoff and landing conditions at different pressures.

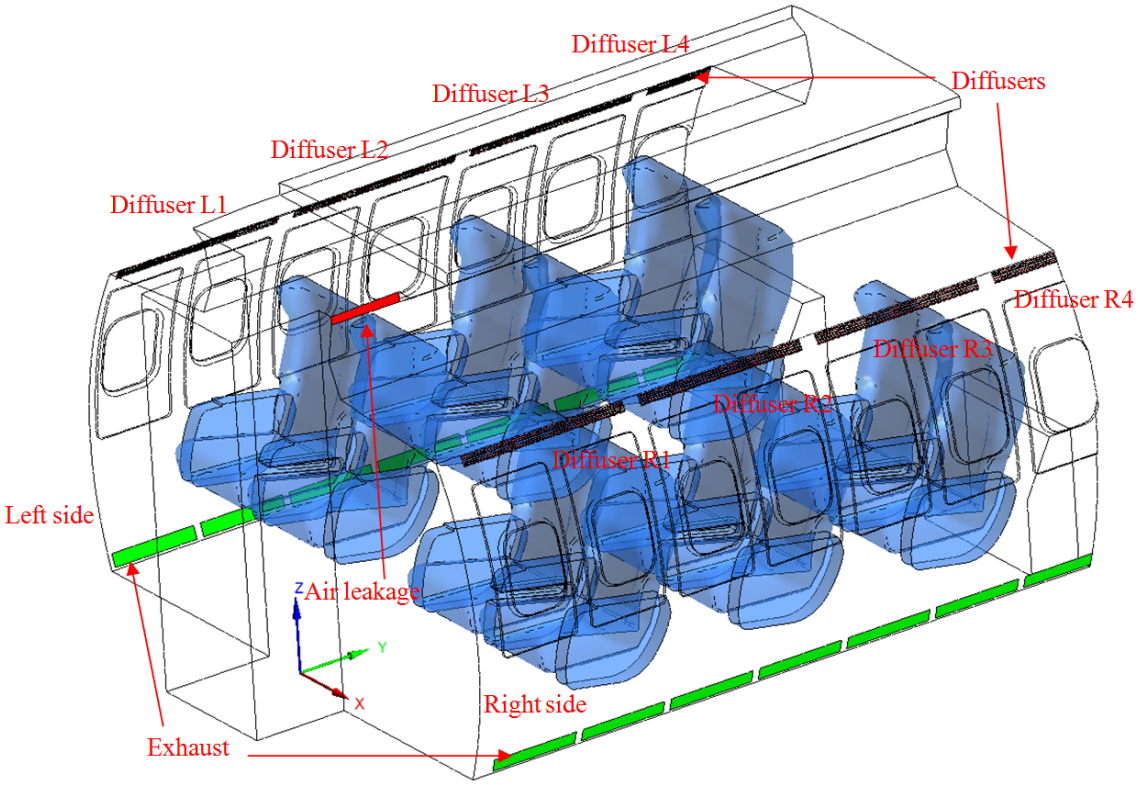

Figure 1 Schematic model of the first-class cabin in the MD-82 aircraft.

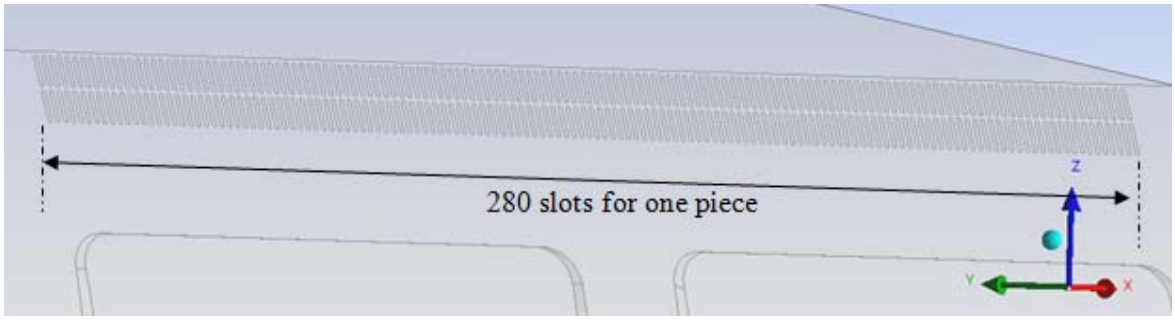

Figure 2 One piece of diffuser that has 280 linear slots arranged in two rows

3. Measuring technique

Numerical simulations by CFD need accurate cabin geometry and boundary conditions from the diffusers such as air velocity and direction. The validation of the CFD results requires high-resolution flow fields in the cabin, such as air velocity, direction, and turbulence. Therefore, the accuracy of the anemometers for the measurements is very crucial. This section discusses the measuring technique for obtaining the cabin geometry, boundary conditions, and flow fields.

3.1 Cabin geometry

This investigation used a laser tracking system and inverse engineering to generate a digital model of an MD-82 aircraft cabin. The whole procedure consisted of four parts: laser scanning, pre-processing, segmentation, and surface fitting.

The laser scanning used a Leica LTD800 tracker scanning system for obtaining the

geometric cloud of the MD-82 cabin. The system consisted of a T-scan based on a non-contact method and a T-probe, which was a contact sensor as shown in Figure 3. Generally, most of the point cloud can be obtained by a T-scan. Objects such as exhausts that could not be accessed by the laser beam could not be measured by the T-scan and so must be measured separately by the T-probe. Laser scanning of the geometry can generate high density clouds that reflect in an informative way the geometrical structure of a measured object.

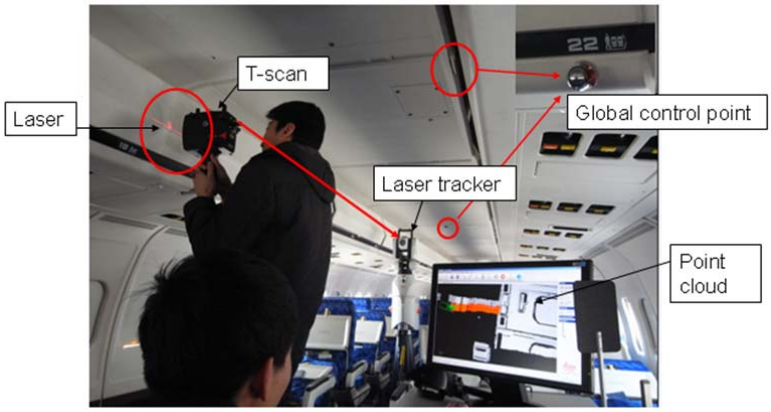

Figure 3 The laser tracking system with T-scan in the cabin

Preprocessing of cabin scanning data and rectification of the same coordinates are the most important processes in reverse engineering. In a narrow space such as an airliner cabin, the scanner must be moved around to capture the data. And it is necessary to combine these data in the same coordinate, which can be difficult in some circumstances. For example, when we scanned the cabin, the wind was so strong that the cabin swayed slightly. The coordinates of the cloud data moved to some extent. After more than 20 years in service, the cabin geometry was distorted, so the reading from the original design could not be accurate. All these factors must be carefully considered in the pre-processing of the cloud data.

The segmentation was to select useful points and to discard noisy points in the cloud data for forming simple surfaces. The segmentation can be edge-based or face-based. This investigation used the edge-based segmentation since it is relatively easy to operate. The method found the boundary of every simple surface and picked up the point data on the boundary.

Surface fitting is to select data points at the boundaries of a simple surface, e.g., a plane, a cylinder, and a sphere and then link the two adjacent surfaces. If there are gaps between the surfaces and the data cloud, they need to be approximated to fit the surface. A CAD model of a cabin can be finally assembled with those surfaces.

3.2 Calibration of instrument

As shown in Figure 2, the air diffusers were very complicated and in a real airplane the cabin wall was not transparent. Optical methods such as PIV, PTV, and PSV are not appropriate for this investigation. Therefore, our investigation used point anemometers.

The first step in air velocity measurements was to calibrate the anemometers. According to the flow speed, this study used two types of anemometers, HSA and UA. The HSA was based on Newton's law for cooling to obtain the velocity. A higher air velocity can cool down the heated probe so the air velocity can be determined from the temperature of the probe. As the probe was held by a stick, the cooling effect might have been different if the flow had been approached from a different angle. It is thus important to study the sensitivity

of the probe towards the flow angle.

This investigation used a UA as a reference which could provide accurate velocity and direction for the flow from a diffuser. The measuring accuracy of UA is ±2% of absolute value of indicated value and measurement range is 0~10 m/s with the measuring resolution of 0.005 m/s. As shown in Figure 4, a UA was used to measure the velocity at points A, B, and C on a diffuser outlet. The jet was discharged horizontally with a velocity of 3.119, 3.008, and 3.047 m/s, respectively, at the three locations as measured by the UA. Figure 5 shows the measured velocity components at point A. The figure shows the velocity components at the three directions and the velocity magnitude for 240 s. The results confirmed that the discharge velocity was horizontal because V_x and V_z were close to zero. The turbulence intensity was not very high (6.4%). Then, three identical HSAs were employed to measure the air velocity at A, B, and C with different measuring angles, α. The measurement range of HSA is 0.05~5 m/s with measuring accuracy of 0.02 m/s. As shown in Figure 4, the angle varied from 0 to 90 degrees so one can test if the probe is omni-directional, as claimed by the manufacturer. Figure 6 shows that, when α was small (between 0-15^o), the averaged velocities at A, B, and C were 2.92, 2.94, and 2.88 m/s, respectively. The velocities measured by the HSAs were close to those measured by the UA. When α was larger than 15^o, the measured velocity varied at different points and showed large discrepancies with those measured by the UA. Therefore, the measuring angle α should be less than 15^o.

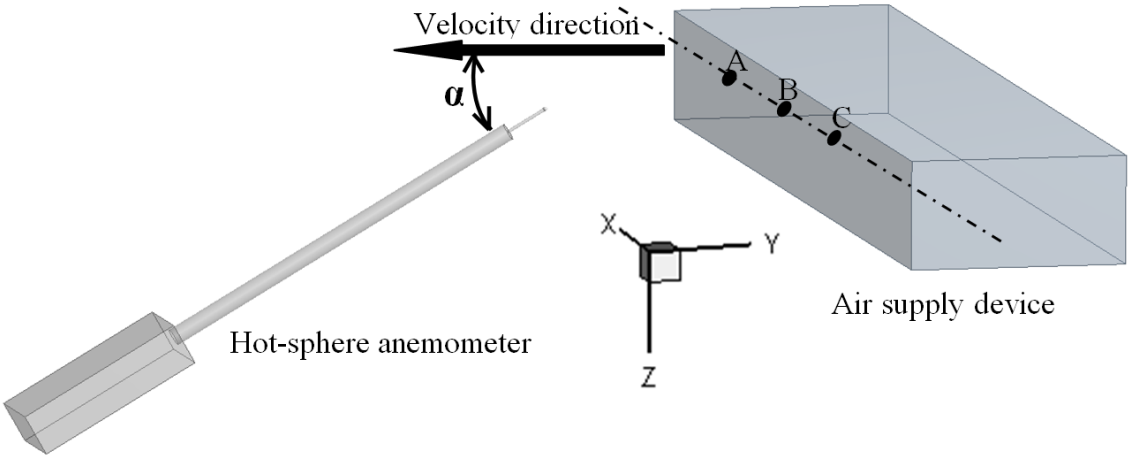

Figure 4 Setup for testing the measuring angle of the HSAs

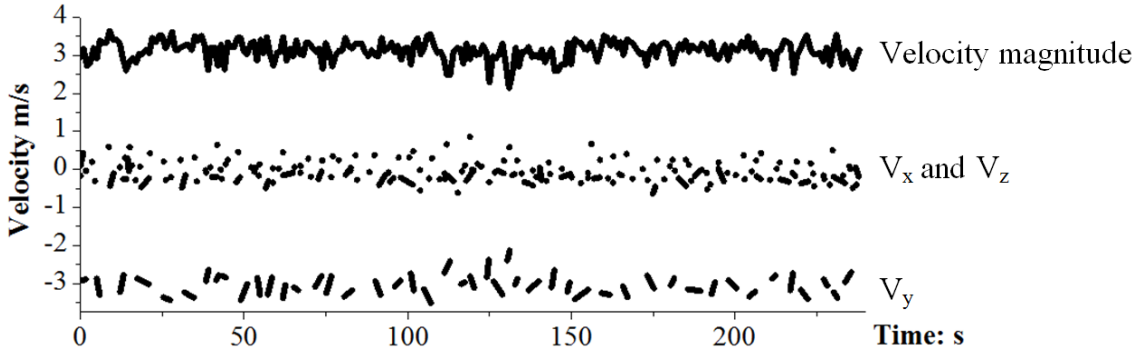

Figure 5 Measured velocity at point A by the UA

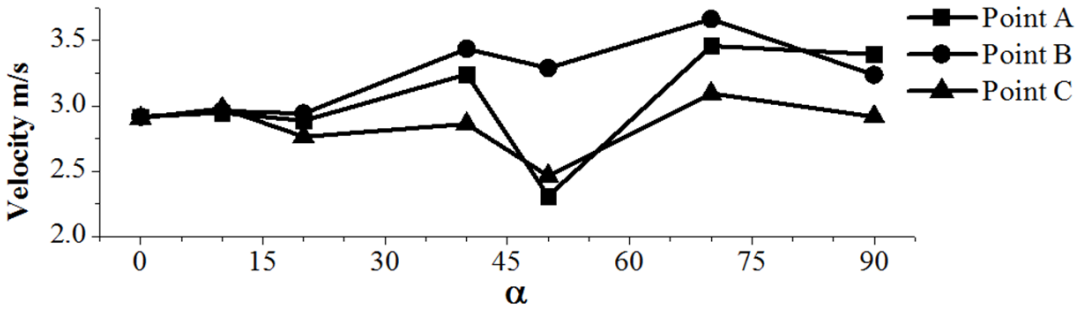

Figure 6 Measured velocities at A, B, and C by the HSAs with different measuring angles

3.3 Airflow boundary conditions on the diffusers

With the calibrated HSAs, the velocity on the upper row of a diffuser was measured at five different heights on each slot as shown on the right of Figure 7. As the probe of an HSA (with a diameter of 2 mm) was smaller than the slot, it could be placed very close to the slot to obtain the true supply air velocity. The results shown in Figure 7 indicate that the flow was discharged uniformly at different heights on each slot. It was sufficient to measure only one representative velocity on each slot. However, Figure 7 also shows that the velocity varied greatly from one slot to another. Note that the air velocity at most of the slots was higher than 0.5 m/s. The HSAs should be sufficiently accurate since the impact of the natural convection from the probes was insignificant.

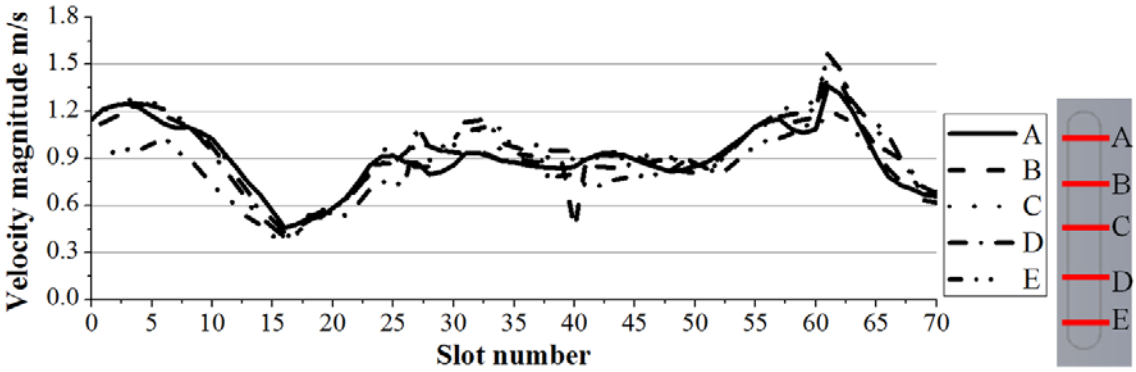

Figure 7 Measured velocity magnitude at different heights of slot with HSA

Unfortunately, the HSAs could not measure the flow direction, which is a very important boundary condition. This investigation used UAs to measure the flow direction as a supplement. Due to the large size of its probe, the UA could not be placed close to the air supply slots as shown in Figure 8(a). This study placed the UA as close as possible to the slots so that the velocity direction could be measured as shown in Figure 8(b).

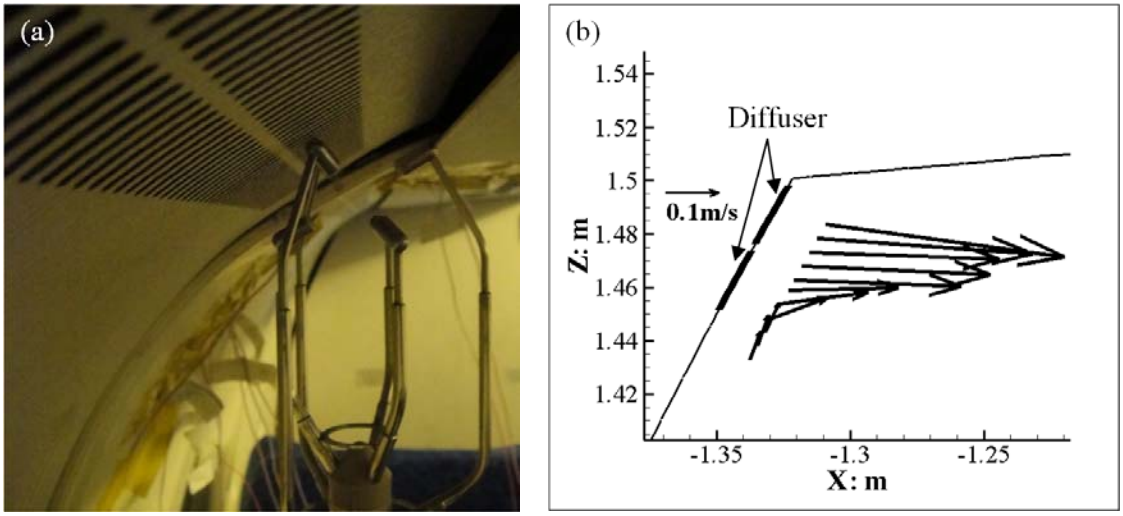

Figure 8 (a) Setup of UA, (b) Measured velocity direction by the UA at locations close to the diffuser

Since the velocity varied greatly from one slot to another, one cannot use the measurement at one slot to represent the one at another slot. Therefore, for velocity magnitude measurements, several HSAs were clustered on a supporting device that could be moved horizontally to measure the velocity at multiple slots as depicted in Figure 9(a). The distance between the probes and slots was about 4 mm. The measurements at one position were performed for 30 s before moving on to the next one. For velocity direction, the UAs were used in a similar manner as illustrated in Figure 9(b). The probe of UA was placed at the upper slots and each measurement lasted for 20 s. The distance between the center of probes and slots was about 15 mm. All the measurements were repeated at least once.

Figure 9 Instrument setup: (a) HSAs and (b) UAs

3.4 Airflow field

This investigation used 9 UAs to obtain the three-dimensional air velocity distribution in the cabin. As UAs provide point-by-point data, to increase the resolution of the measured flow field, they were moved manually from one location to another. After the movement of the UAs, the flow field needs to be stabilized before taking the measurements.

To develop a reliable measuring procedure, this investigation first measured the air velocity at seven different locations, as shown in Figure 10, which could represent different flow regimes in the cabin. The measurement started immediately after the UAs were placed at those positions. This study first measured the air velocity at those locations for one hour at 20

Hz and produced 72,000 data for each velocity component at a location. Figure 11 shows the measured instantaneous velocity magnitude at a typical position (position 2) between 0~60 min; it is impossible to tell when the flow field would be stable. Therefore, the data was analyzed by comparing the averaged velocity and turbulence intensity between 0~2, 0~4, 0~6, 0~8, 0~10, 0~12, 0~14, and 0~16 min with those between 16~60 min. The results show that, at the seven locations, the differences between 0~8 min and 16~60 min can differ as much as 3.8% to 20% for velocity and 0.4%~7.3% for turbulence intensity. Figure 12 compares the results at position 2 showing that the system stabilized after 8 min when UAs were placed in the right positions.

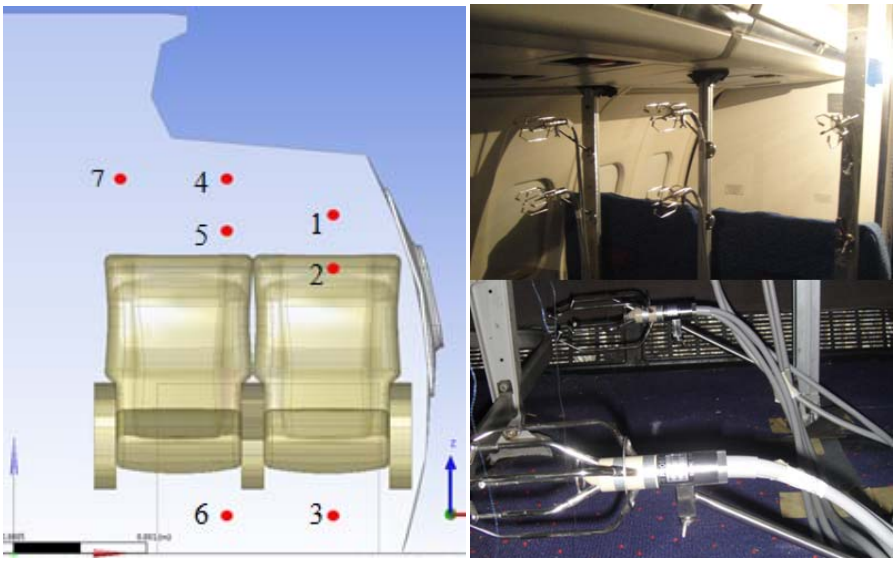

Figure 10 Locations of the sampled points for stability time test

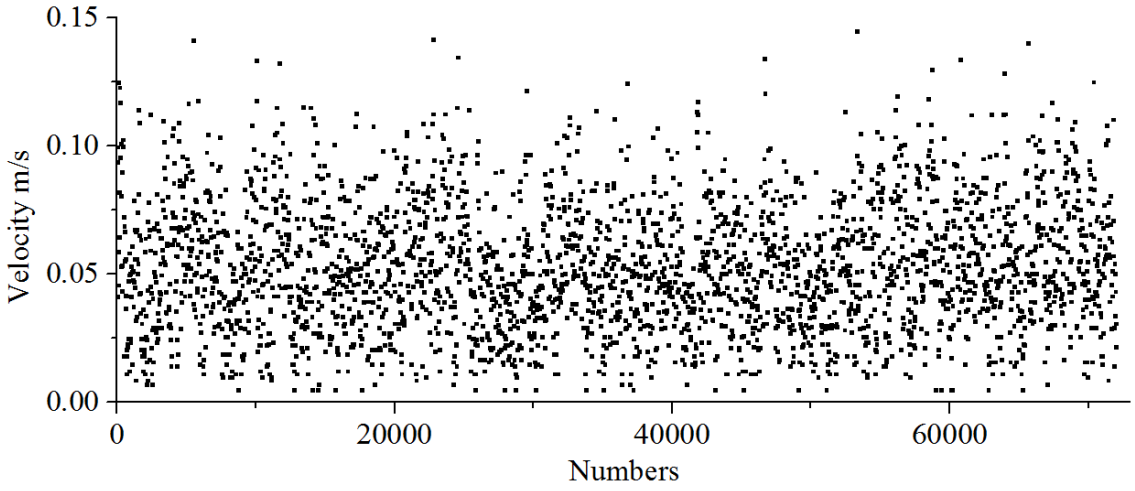

Figure 11 Measured instantaneous velocity magnitude at position 2 between 0~60 min

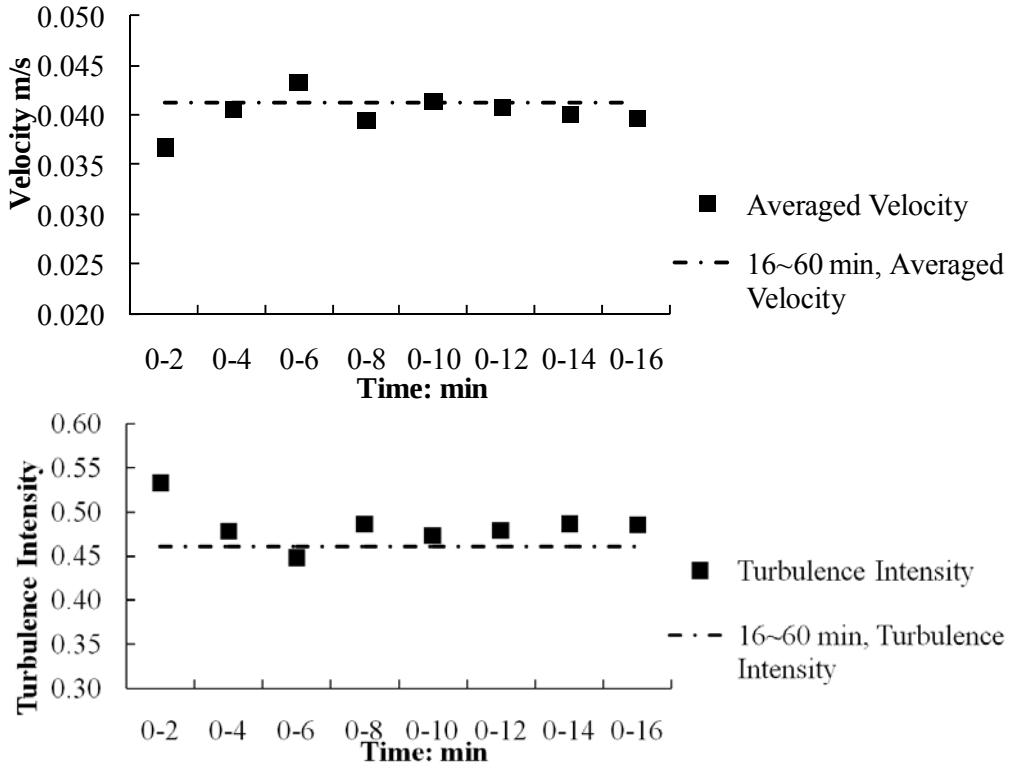

Figure 12 Comparison of the averaged velocity and turbulence intensity between 0~2, 0~4, 0~6, 0~8, 0~10, 0~12, 0~14, and 0~16 min with those between 16~60 min at position 2

To study the time needed to obtain accurate averaged velocity and turbulence intensity, the data was further analyzed by comparing the averaged velocity and turbulence intensity between 8~9, 8~10, 8~12, 8~16, 8~24, and 8~40 min with those between 8~60 min. The results show that the differences between the data of 8~12 min and those of 8~60 min were as few as 1.7% to 9.1% for velocity and 0.2%~5.9% for turbulence intensity at the seven locations. Figure 13 shows a comparison at position 2, which represents a typical location. The mean data obtained between 8~12 min were sufficiently accurate for the averaged velocity and turbulence intensity.

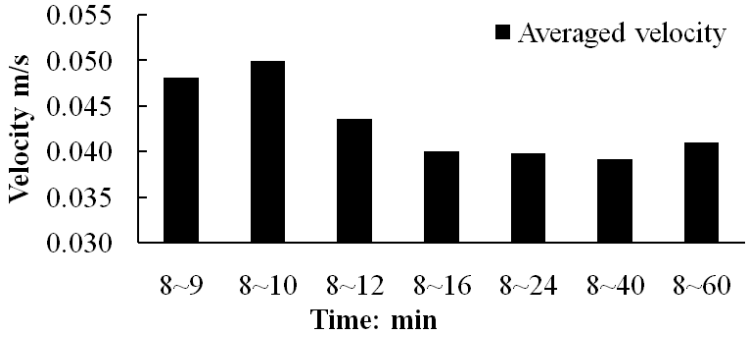

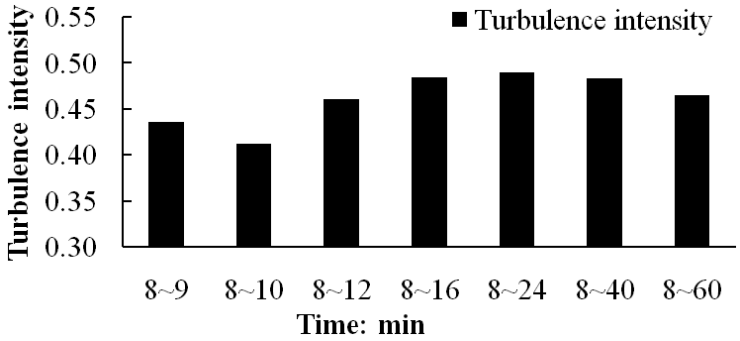

Figure 13 Comparison of the averaged velocity and turbulence intensity between 8~9, 8~10, 8~12, 8~16, 8~24, and 8~40 min with those between 8~60 min at position 2

To have a comprehensive overview of the air distribution in a cabin, this investigation measured the airflow in three cross sections as well as three longitudinal sections (window seats, aisle seats, center of the aisle) as shown in Figure 14. These sections would provide different airflow characteristics in all the important spaces in the cabin. Since we had only nine UAs, they were fixed in two supporting sticks, and the sticks can be moved both vertically and horizontally to reach those six sections. Each UA generated 4800 data entries of each instantaneous velocity component in 4 minutes (20 Hz × 240 s for one velocity component). With the three-dimensional instantaneous velocities, turbulent intensity and turbulent kinetic energy could be further calculated. The measuring resolution was 0.1 m along the height and 0.1 m along the width for the cross sections, and 0.1 m along the height and 0.2 m along the width for the longitudinal sections. It would not be meaningful to have a resolution finer than 0.1 m because the sensor size was 0.03 m in diameter. In the first-class cabin with a complicated geometry, the resolution led to a total of 343 measuring points for each cross section and 304 measuring points for the longitudinal section along the aisle. This investigation repeated the measurements at least once.

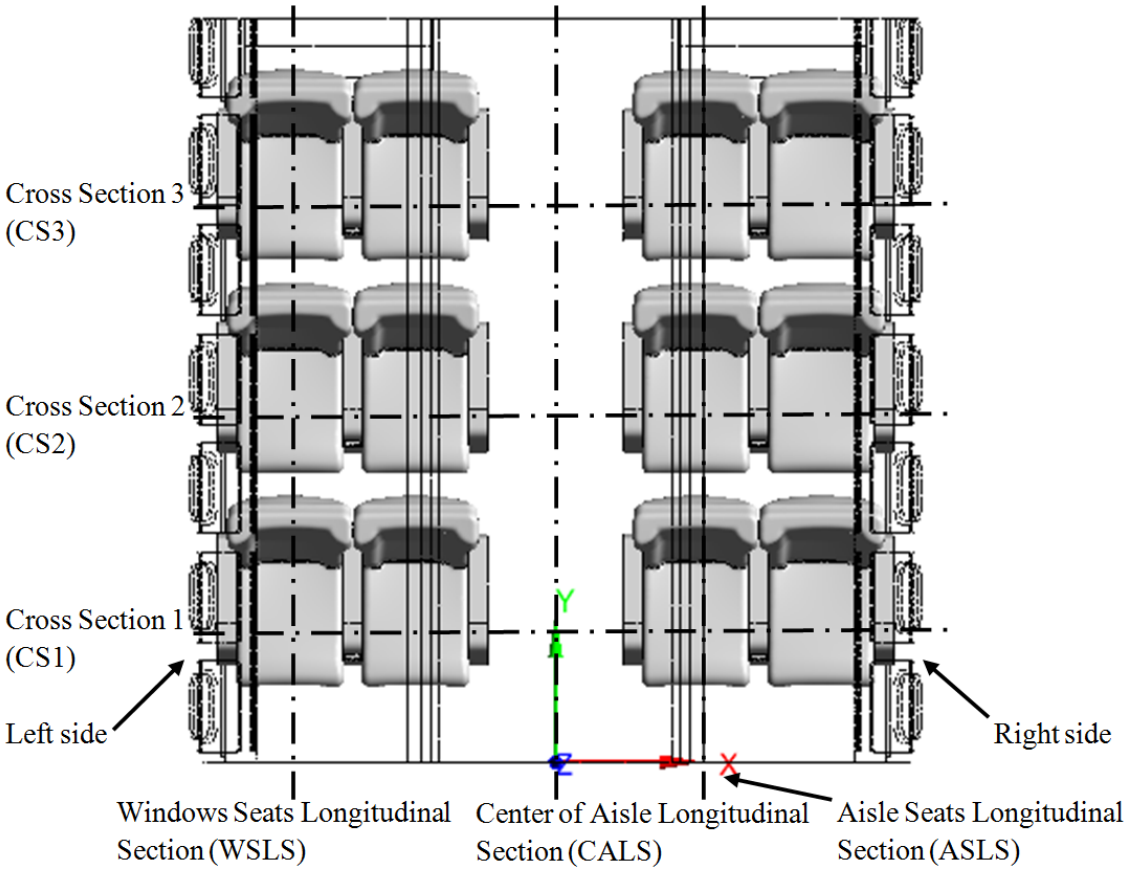

Figure 14 Plane view of measured sections in the first-class cabin

4. Results

4.1 Cabin geometry

Figure 15(a) shows a typical cabin cross-section obtained by using the cloud data from the scanning. The details, such as the window, can also be generated from the cloud data as shown in Fig. 15(b). Such a section as the window can be used to construct the whole fuselage, as shown in Fig. 15(c). Figure 1 is actually the detailed geometry of a first-class cabin generated from the scanning. A digital model is needed for the CFD simulations to generate meshes. By using the model, our investigation found the first-class cabin air volume to be 15.484 m^3.

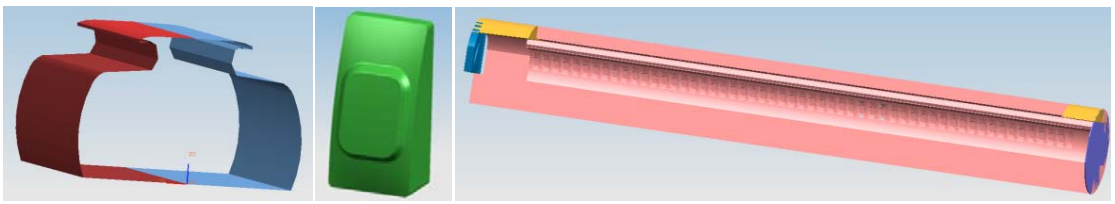

(a) A typical cabin section (b) A window (c) Whole cabin fuselage

Figure 15 Generation of a digital model for the cabin fuselage

The global shape accuracy of the digital model, U_g, can be determined from:

$$U_g = \sqrt{U_{ss}^2 + U_{gs}^2 + U_{st}^2}$$

where U_{ss} is the local measuring precision between the spot and the laser tracker, U_{st} is the local measuring precision between the T-scan and the laser tracker and U_{gs} is the global measuring precision between the laser tracker and the global control system. The deviation of the laser tracker was 6 μm/m with a basic deviation of ±15μm and the deviation of the T-scan was 2 μm/m with a basic deviation of ±20 μm. Leica LTD800 can work with nanometer accuracy, which is not necessary for the low density of point clouds in this case. Taking the economy-class cabin for example, the distance between the tracker and spot was 5 m, between the tracker and global control was 30 m and between the T-scan and laser tracker was 5m. Thus the global shape accuracy, U_g, can be obtained to be only 202 μm by using U_{ss}=15 μm + 6 μm/m × 5 m = 45 μm, U_{gs} =195 μm, and U_{st} = 30 μm.

4.2 Air velocity from the diffusers

Figure 16 shows the measured velocity magnitude along the diffuser on both sides including upper and lower slots. The data from the repeated measurements agreed well with each other. The velocity magnitude varied greatly from one slot to another and the supply air was asymmetrical. Comparing the velocity profile of the diffuser upper slots with that of the lower slots, the two velocity profiles were not exactly the same. Thus, it is necessary to measure the velocity in both rows of diffusers.

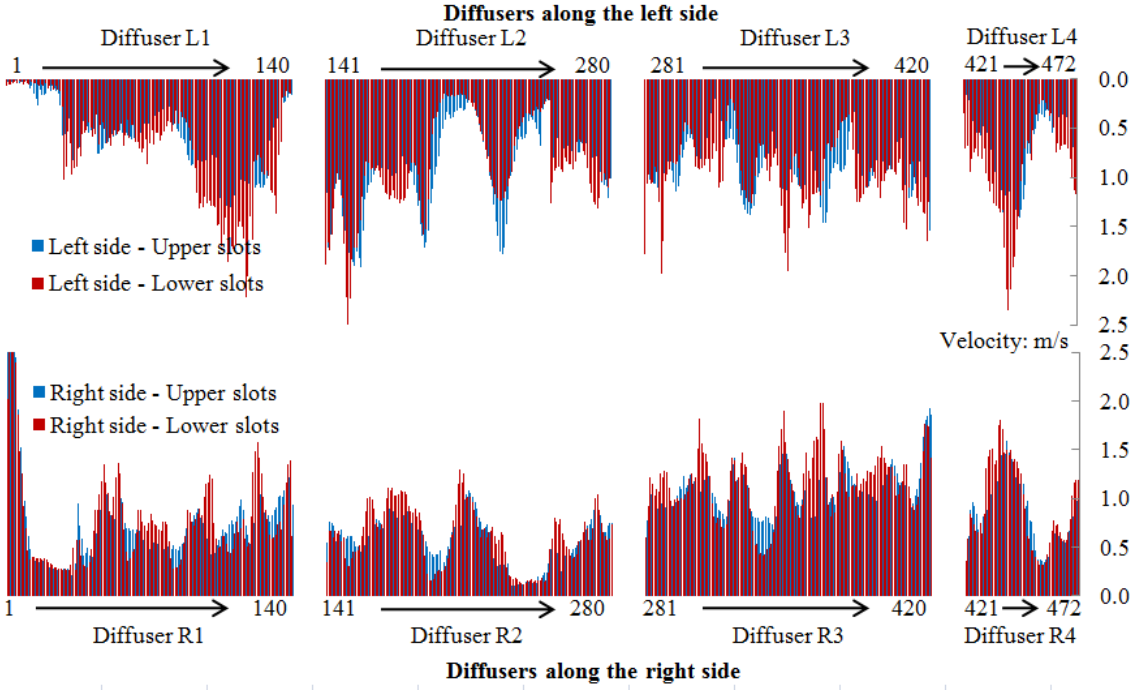

Figure 16 The air velocity profile measured by HSAs (left or right is referred to in Figure 14, upper or lower refers to the upper row or lower row of the diffuser slots)

UAs were also used to measure the supply air velocity profiles along the diffusers. Figure 17(a) compares the measured velocity profile by the UAs with that by the HSAs at one of the diffusers. The two velocity profiles were alike but the velocity measured with the UAs was much lower due to the jet decay from the slots to the UA probe. This study assumed that the velocity direction would not change much from the slots to the probe positions due to the

small distance. Then the velocity direction measured by the UAs can be regarded the same one as in the slots. Figure 17(b) compares the turbulence kinetic energy measured by the HSAs with that by the UAs. The results by the UAs were lower than those measured by the HSAs. Since the UAs were placed a little far away from the slots, the turbulent energy decayed from the slots to the probes. By studying the velocity components measured by the UAs (Figure 17(c)), V_y was the lowest showing the two-dimensionality of the cabin flow but the V_y was not absolutely zero. The longitudinal flow should not be neglected.

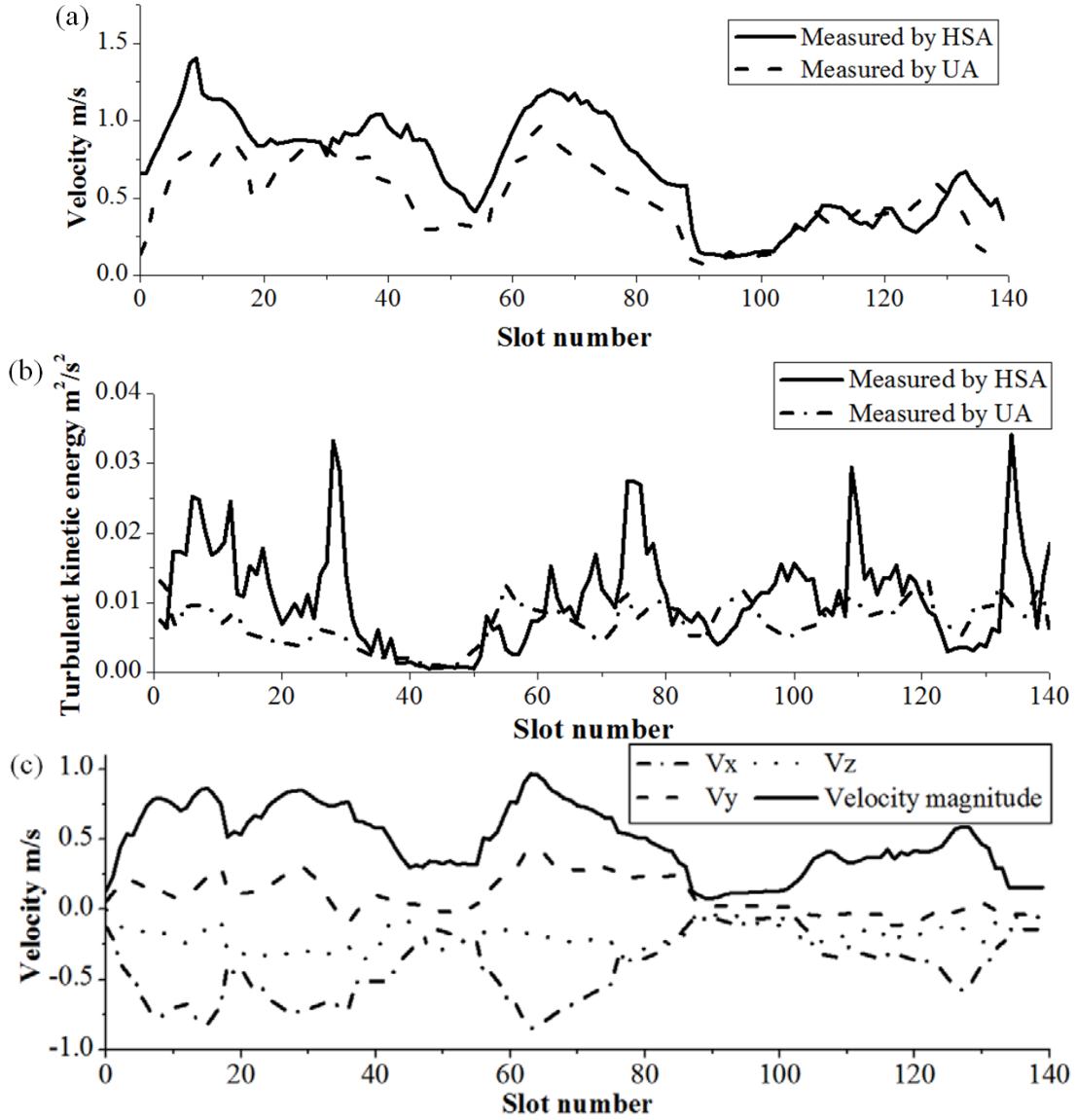

Figure 17 (a) Comparison of the measured velocity profiles by the HSAs and UAs along the diffusers, (b) Comparisons of the measured turbulent kinetic energy by HSA and UA, and (c) Measured 3-dimensional velocity with UA

4.3 Airflow field

The airflow field was measured twice for each section under isothermal conditions. The two measurements were at least one week apart to ensure the repeatability of the boundary conditions and the airflow patterns. For example, Figure 18 compares the measured

velocity vectors in section CALS, which was a typical section. The results show that the two sets of results were almost identical.

Figure 19 depicts the velocity distributions in the three cross sections and three longitudinal sections. The air supply from the diffusers from the two sides of the cabin created two large recirculations on each side of the cabin, which was the original design intention. The two air jets from the diffusers merged at the aisle and separated again near the floor. One part of the flow was extracted from the exhausts on the sidewalls near the floor and the rest was recirculated due to the momentum effect. Please note that the airflow was not symmetrical due to the asymmetrical air supply and unexpected flow in the upper part of the cabin (Figure 19(a)). The spaces on the section through the aisle seats were in the downward flow region, while the spaces through the window seats were in the upward flow region created by the two large recirculations.

The contours in Figure 19 also show the velocity in the longitudinal (y) direction for the cross sections. There was a significant longitudinal flow in the upper part of the cabin (positive y direction). The longitudinal flow can be clearly seen from the air velocity distributions in the longitudinal section at the center of the aisle and cross section at the first row (Figures 19(a) and 19(b)). This unexpected longitudinal flow was caused by air leakage (Figure 1) that was further located by an infrared camera (Figure 20). A UA was applied to measure the boundary conditions of the air leakage, and the air leakage rate was 15.8 m^3/h.

Among the 1625 points measured, Figure 21 illustrates that 72% of the points had a velocity lower than 0.1 m/s. Thus, the flow field in this empty cabin was at low speed. Since the velocity was measured by the UA, it should be accurate.

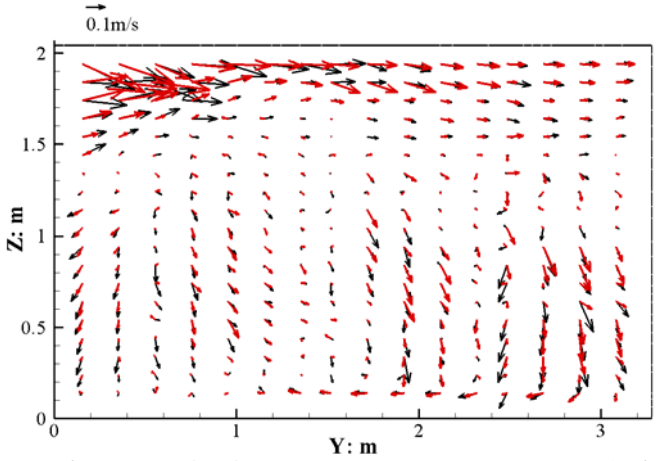

Figure 18 Comparison of measured velocity vectors in section CALS (referred to in Figure 14)

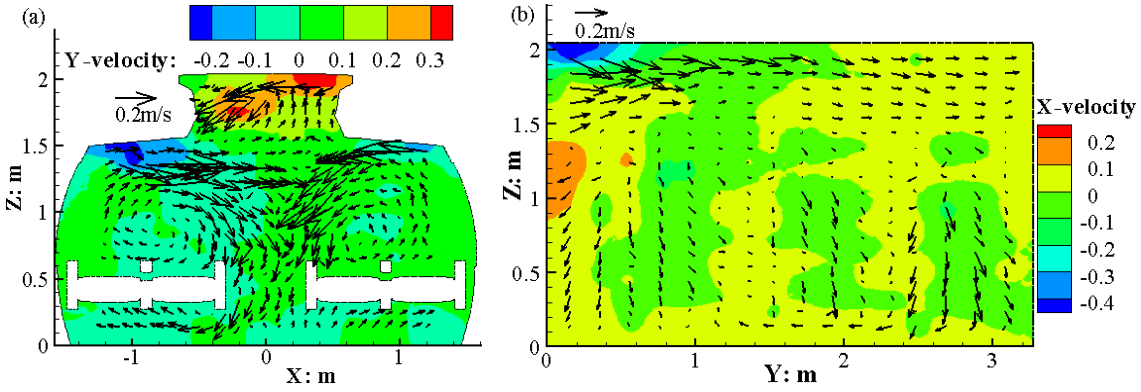

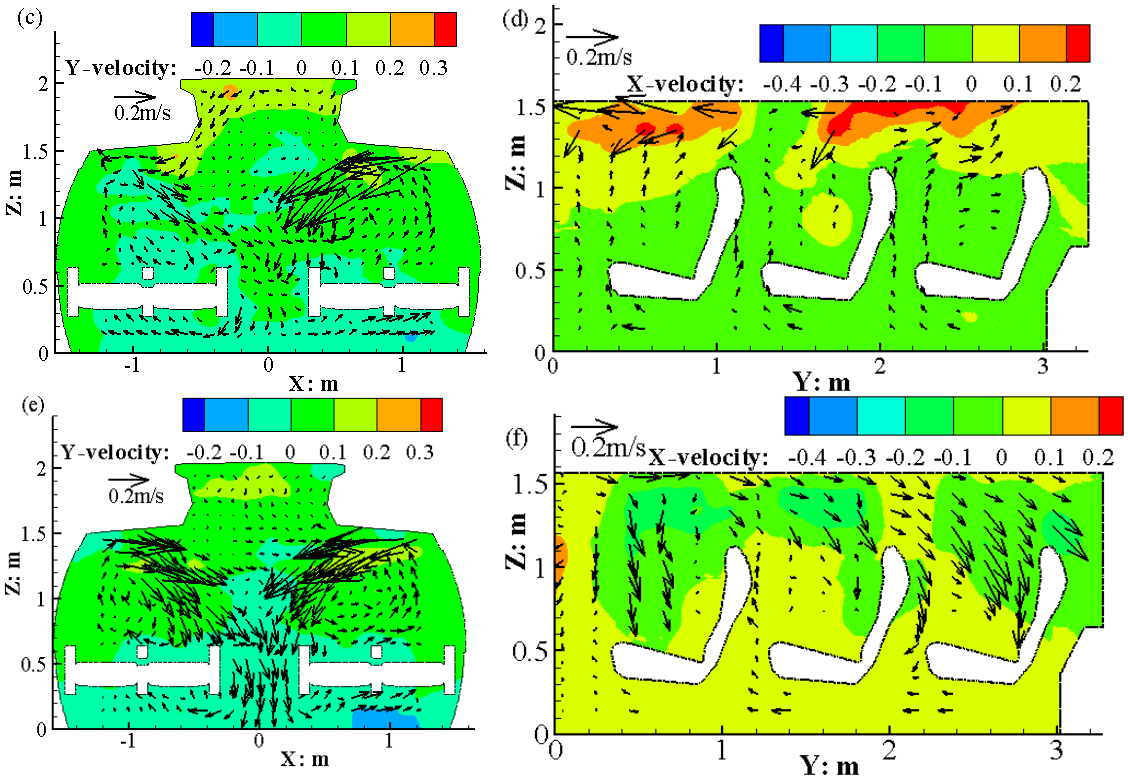

427 *Figure 19 Measured flow field: (a) CS1, (b) CALS, (c) CS2, (d) WSLS, (e) CS3, and (f) ASLS*
428 *(All the locations are referred to in Figure 14)*
429

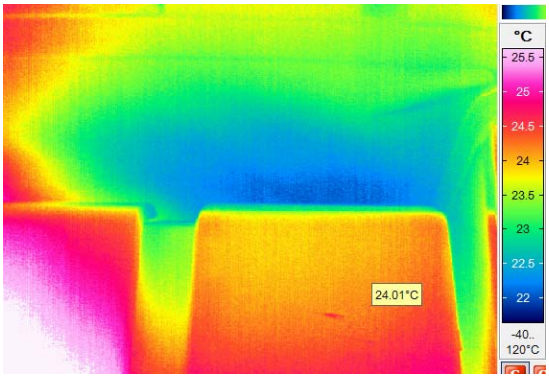

Figure 20 Localization of air leakage by infrared camera

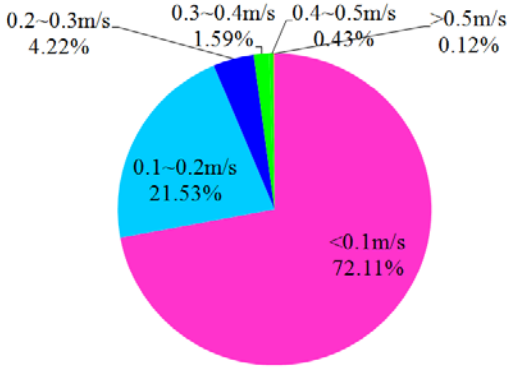

Figure 21 Distribution of velocity magnitude of all measured 1625 points

430
431 Figures 22(a), 22(c), and 22(e), respectively, show the turbulent kinetic energy (TKE)
432 in three cross sections. The TKE near the diffusers was pretty high, but decayed along the
433 airflow path and in the recirculation zones. Obstacles in the cabin, such as armrests, would
434 increase the local TKE. Although the TKE in the recirculation zones was low, the turbulence
435 intensity was high, as shown in Figures 22(b), 22(d), and 22(f), respectively, because of the
436 low air velocity in the zones.
437

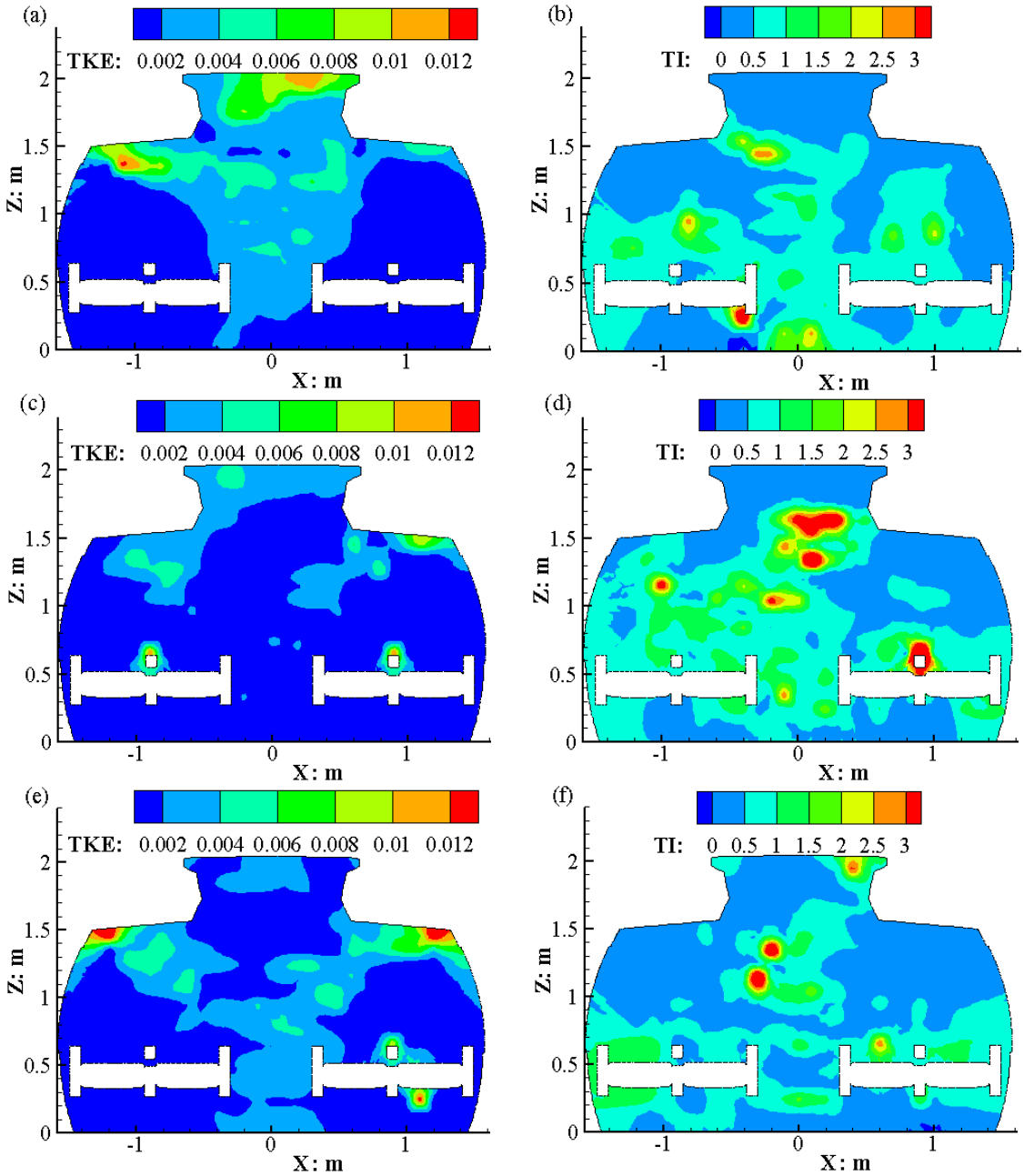

Figure 22 Distributions of turbulent kinetic energy (TKE) at sections (a) CS1, (c) CS2, respectively, and (e) CS3 and those of turbulence intensity (TI) at sections (b) CS1, (d) CS2, and (f) CS3, respectively

5. Discussion

This investigation also measured the air flow rate by the constant tracer gas method and found that the flow rate was 565 ± 15 m^3/h. The air flow rate can also be calculated by summing up the airflow rate of each slot:

$$Q = \sum_{All\ slots} v_i \times S \times \cos\alpha$$

where Q (m^3/h) is the airflow rate; v_i (m/s) is the measured velocity for slot i; S (m^2) is the area of each slot; and α is the incident angle of the velocity direction normal to the slot. The calculated air flow rate was only 339.8 m^3/h. Since the HSAs could not be placed very close to the slots, the difference might be caused by the rapid velocity decay from the slots to the HSA probes.

To study the velocity decay from the slots, this study used CFD with the RNG k-ε model to predict the airflow near the diffuser region. For simplicity, this investigation calculated only half of a small section of empty cabin as shown in Figure 23(a) and applied symmetrical conditions in the middle and periodic conditions on both ends to reduce the computing effort. The computational domain included the thickness of the air supply slot that was 5 mm. The supply flow rate was that measured by the tracer-gas method. This section of the cabin contained 140 diffuser slots, Figure 23(b) shows the velocity decay profile from three typical slots. the air velocity decayed significantly from the inner face of the diffuser slots. The HSA probes were placed about 4 mm from the inner face, the velocity decayed by 31% - 34%, By using HSA data without considering its decay, the flow rate was estimated 339.8 m^3/h. By considering the decay, the flow rate would be 510 m^3/h that is close to 565 m^3/h as measured by the tracer gas method. This has indirectly verified the reliability of the tracer-gas method.

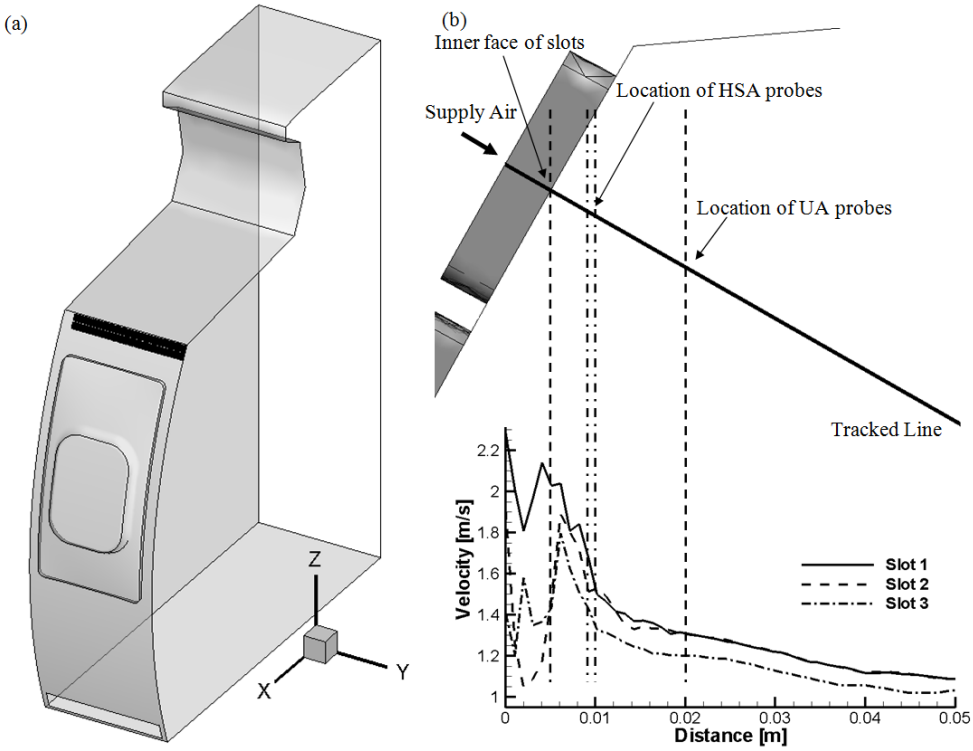

Figure 23 (a) Sketch of calculated domain; (b)CFD predicted velocity decay of the jet from the slots.

Therefore, one can use the airflow rate from the tracer-gas method, the measured velocity by HAS with 32% scaling up, and the measured velocity direction by UA, to give an accuracy inflow boundary condition. For CFD simulations, the mesh size at the diffuser region should be less than the width of the slot (3 mm). In addition, our investigation measured the air velocity by UA and HSA with a frequency of 20 Hz and 8 Hz, respectively. The turbulence information measured could be used as input for Reynolds-averaged Navier-

Stokes (RANS) models and Detached Eddy Simulations (DES). Large Eddy Simulations (LES) could use no perturbations, spectral synthesizer methods to prescribe fluctuating velocity at the diffuser slots. The measured data has sufficient information needed. Hence, the data for the diffuser slots from this investigation is sufficient for CFD simulations by RANS, DES, and LES.

6. Conclusion

This investigation described a procedure to obtain high-quality cabin geometry, boundary conditions at the diffusers, and flow fields in the first-class cabin of a functional MD-82 commercial airliner. The study led to the following conclusions:

High quality cabin geometry can be obtained by using a laser tracking system with reverse engineering.

By combing HSAs and UAs, this study could obtain velocity magnitude, velocity direction, and turbulence intensity at the diffusers. The boundary conditions in the airplane were very complex.

UAs can be used to accurately measure the distributions of three-dimensional air velocity, turbulent kinetic energy, and turbulence intensity. The air supply from the diffusers from the two sides of the cabin created two large recirculations on each side of the cabin. The airflow was not symmetrical due to the asymmetrical air supply and unexpected flow in the upper part of the cabin. The turbulence kinetic energy in the recirculation zones was low, because of the low air velocity in the zones. However, the turbulence intensity was high. The measurement found significant longitudinal flow in the cabin.

Acknowledgement

The research presented in this paper was financially supported by the National Basic Research Program of China (The 973 Program) through grant No. 2012CB720100.

References

Chao, J., Mu, X., Liu, W., Wu, H.J., Liu, J., Chen, Q., 2011. Rapid construction of a three-dimensional digital geometric model of an airliner cabin for CFD simulations. Proceedings of the 12th International Conference on Air Distribution in Rooms, ROOMVENT 2011, Trondheim, Norway.

Chen, F., Brown, G.M., Song, M., 2000. Overview of three-dimensional shape measurement using optical methods. Optical Engineering 1(39), 10-22.

Garner, R.P., Wong, K.L., Ericson, S.C., Baker, A.J., Orzechowski, J.A., 2003. CFD validation for contaminant transport in aircraft cabin ventilation flow fields. Proceedings of Annual SAFE Symposium on Survival and Flight Equipment Association, 248-253.

Günther, G., Bosbach, J., Pennecot, J., Wagner, C., Lerche, T., Gores, I., 2006. Experimental and numerical simulations of idealized aircraft cabin flows. Aerospace Science and Technology 10(7), 563-573.

Liu, W., Mazumdar, S., Zhang, Z., Poussou, S.B., Liu, J., Lin, C.-H., Chen, Q., 2012. State-of-the-art methods for studying air distributions in commercial airliner cabins. Building and Environment 47, 5-12.

Marcus, R., Rolf-Rainer, G., 2010. Segmentation and classification of streaks in a large-scale particle streak tracking system. Flow Measurement and Instrumentation 21, 1-7.

Mo, H., Hosni, M., Jones, B., 2003. Application of particle image velocimetry for the measurement of the airflow characteristics in an aircraft cabin. ASHRAE Transactions

529 109(2), 101-110.
530 Space, D.R., Johnson, R.A., Rankin, W.L., Nagda, N.L., 2000. The airplane cabin
531 environment: Past, present and future research. ASTM Special Technical Publication
532 1393, 189-214.
533 Sze, T.G.N., Wan, M.P., Chao, C.Y.H., Fang, L., Melikov, A., 2009. Experimental study of
534 dispersion and deposition of expiratory aerosols in aircraft cabins and impact on
535 infectious disease transmission. Aerosol Science and Technology 43, 466-485.
536 Zhang, Y., Sun, Y., Wang, A., Topmiller, J.L., Bennett, J.S., 2005. Experimental
537 characterization of airflows in aircraft cabins, part II: Results and research
538 recommendations. ASHRAE Transactions 111(2), 53-59.
539 Zhang, Z., Chen, X., Mazumdar, S., Zhang, T., Chen, Q., 2009. Experimental and numerical
540 investigation of airflow and contaminant transport in an airliner cabin mockup. Building
541 and Environment 44(1), 85-94.